

Supporting Information

Cerium Oxide Modified Iridium Nanorods for Highly Efficient Electrochemical Water Splitting

Kai Xu,^a Zizeng Zhu,^a Wen Guo,^a Hongyan Zhang,^a Tingting Yu,^a Wenxian Wei,^c Wenjie
Liang,^a Dongen Zhang,^a Maoshuai He,^{*b} and Tao Yang^{*a}

^a School of Environmental and Chemical Engineering, Jiangsu Ocean University,
Lianyungang 222005, Jiangsu, China

^b State Key Laboratory of Eco-Chemical Engineering, Ministry of Education,
College of Chemistry and Molecular Engineering, Qingdao University of Science and
Technology, Qingdao 266042, Shandong, China

^c Testing Center, Yangzhou University, Yangzhou 225009, Jiangsu, China

Correspondence and requests for materials should be addressed to Tao Yang

(yangtao_hit@163.com)

Experimental section

Materials

Iridium chloride hydrate ($\text{IrCl}_3 \cdot x\text{H}_2\text{O}$, 99.8%), potassium iodide (KI, $\geq 99.99\%$), sodium dodecyl sulfate (SDS, 99.0%), polyvinylpyrrolidone (PVP, K30), cerium (III) chloride heptahydrate ($\text{CeCl}_3 \cdot 7\text{H}_2\text{O}$, 99.8%) were all purchased from Aladdin. All the chemicals in the experiments were used as purchased without further purification.

Preparation of Ir/CeO₂ NRs

The Ir/CeO₂ NRs were prepared with a hydrothermal method. Typically, 20 mg of $\text{IrCl}_3 \cdot x\text{H}_2\text{O}$, 170 mg of KI, 150 mg of PVP, 180 mg of SDS and 30 mg of $\text{CeCl}_3 \cdot 7\text{H}_2\text{O}$ were dissolved in 12 mL of deionized water. The resultant homogeneous mixture was stirred in ambient atmosphere at 800 rpm for 10 min. Then the well-dispersed solution was transferred to a 20 mL Teflon-lined stainless autoclave and heated at 180 °C for 24 h in a hot air oven. After cooling to room temperature, the obtained product was collected via centrifugation and rinsed with deionized water at least 3 times, then final product was dried at 80 °C overnight. As contrasts, pure Ir nanorods and CeO₂ nanorods were synthesized by applying a similar synthesis strategy.

Structural characterization

The crystal structures of the as-prepared Ir/CeO₂ NRs electrocatalyst was characterized by powder X-ray diffraction (XRD) conducted on a Bruker D8 Advance X-ray diffractometer (Cu K α radiation, 40 kV, 40 mA). X-ray photoelectron spectroscopy (XPS) was recorded on a Thermo Scientific K-Alpha XPS instrument. Transmission electron microscopy (TEM), high-resolution transmission electron

microscopy (HRTEM), energy dispersive X-ray spectroscopy (EDS) and corresponding elemental mapping were achieved by a FEI Tecnai G2 F30.

Electrochemical measurements

Prior to the measurements, the as-synthesized Ir/CeO₂ NRs (10 mg) were mixed with Vulcan XC-72 carbon (10 mg) in ethanol (10 mL) through ultra-sonication (60 min) and then collected via centrifuge.

The catalyst ink was acquired by adding 5 mg of carbon-supported Ir/CeO₂ NRs into a mixture solution containing 2 mL of water, 1 mL of isopropanol and 25 μL of 5 wt.% Nafion under sonication. Eventually, 15 μL of catalyst ink was transferred onto a pre-cleaned rotating disk electrode (RDE) (diameter: 5 mm). After natural drying under air atmosphere, these as-prepared electrodes were used to test the electrocatalyst performance. For comparison, Ir nanorods were also loaded on carbon support and tested through the same process.

All electrochemical experiments were measured in 1.0 M KOH on an Autolab potentiostat/galvanostat (PGSTAT-302N) workstation with a typical three-electrode cell system at room temperature. RDE, graphite rod and Hg/HgO electrode were used as working electrode, counter electrode, and reference electrode, respectively. The linear sweep voltammetry (LSV) curves were performed at a scan rate of 5 mV s⁻¹ and a rotation speed of 1600 rpm in 1.0 M KOH, and 20 cycles of cyclic voltammetry (CV) tests are operated before the measurements for activation. All applied potentials were switched with respect to the reversible hydrogen electrode (RHE) based on the following equation: $E \text{ (V vs. RHE)} = E \text{ (V vs. Hg/HgO)} + 0.0591 \text{ pH} + 0.098$, and the

overpotential (η) for OER was calculated using the following equation: $\eta = E$ (V vs. RHE) – 1.23 V.¹

For HER measures, the LSVs were subsequently performed at a scan rate of 5 mV s⁻¹ with iR compensation. As for the OER tests, the LSVs were subsequently carried out at a scan rate of 10 mV s⁻¹ with iR compensation. Chronoamperometry was used to evaluate the durability at the overpotential to achieve the constant current density of 10 mA cm⁻². To investigate the electrochemical active surface areas (EASAs), CVs were conducted at various scanning rates (20, 40, 60, 80, 100 mV s⁻¹) to acquire electrochemical double-layer capacitance (C_{dl}) values.² Electrochemical impedance spectroscopy (EIS) measurements were conducted in the frequency range of 0.01 to 10⁵ Hz with an AC amplitude of 5 mV. The electrolyte was bubbled for 30 min with high-purity Ar before each measurement.

Figures

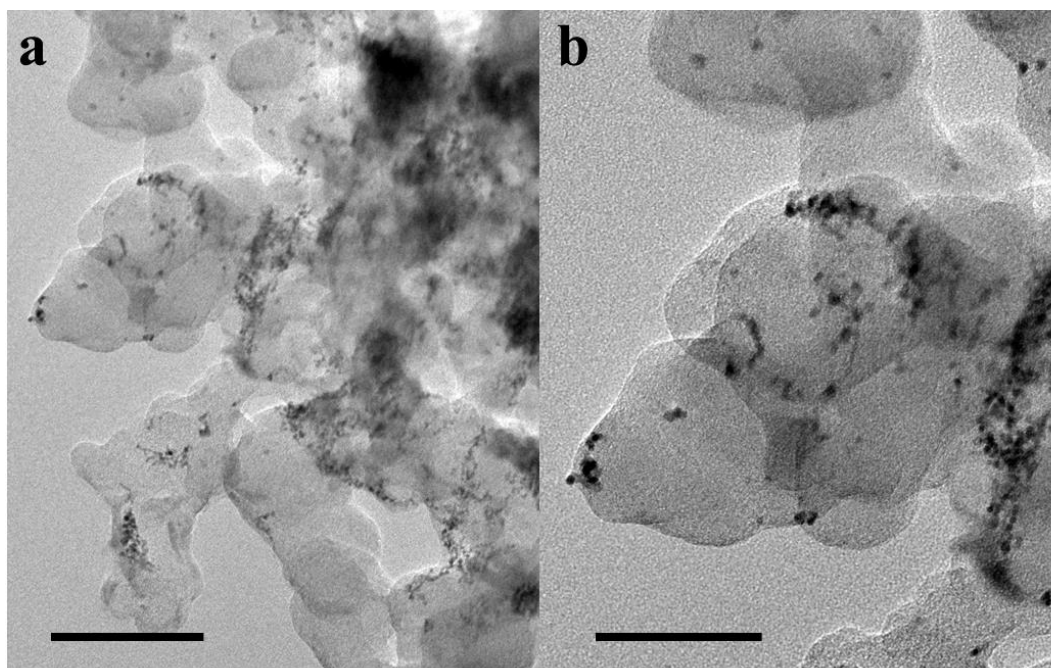


Figure S1 TEM images of the products at (a) low and (b) high magnifications. The scale bars in (a) and (b) are 100 nm and 50 nm, respectively. The Ir nanorods are highly dispersed on the CeO₂ support.

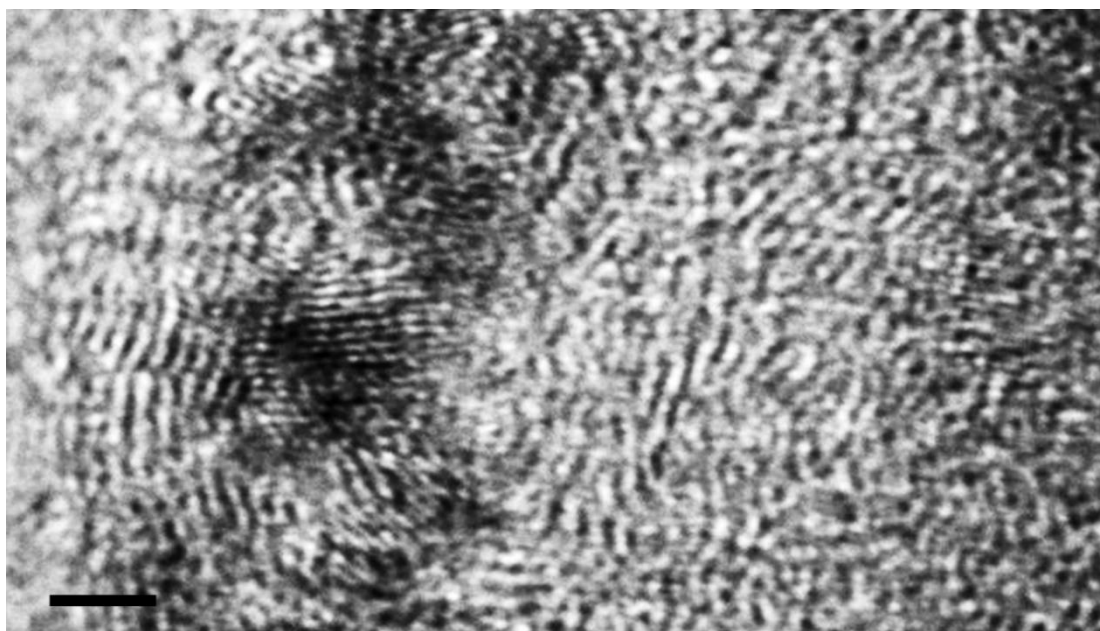


Figure S2 HRTEM of the product. The scale bar is 2 nm. Ir nanoparticles tightly grew on the CeO_2 surface with various orientations.

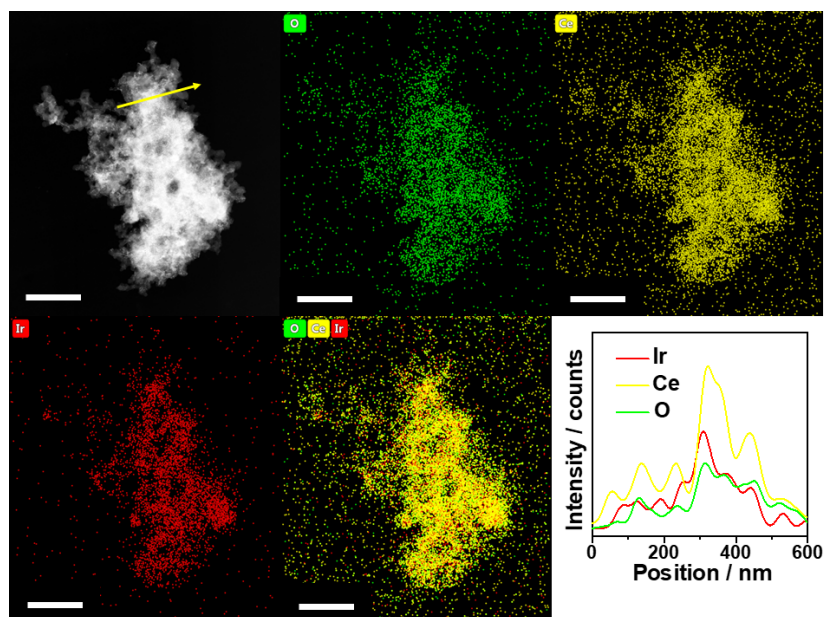


Figure S3 HAADF-STEM image, elemental mapping and EDX cross-sectional compositional line scanning of the product. The scale bar is 500 nm.

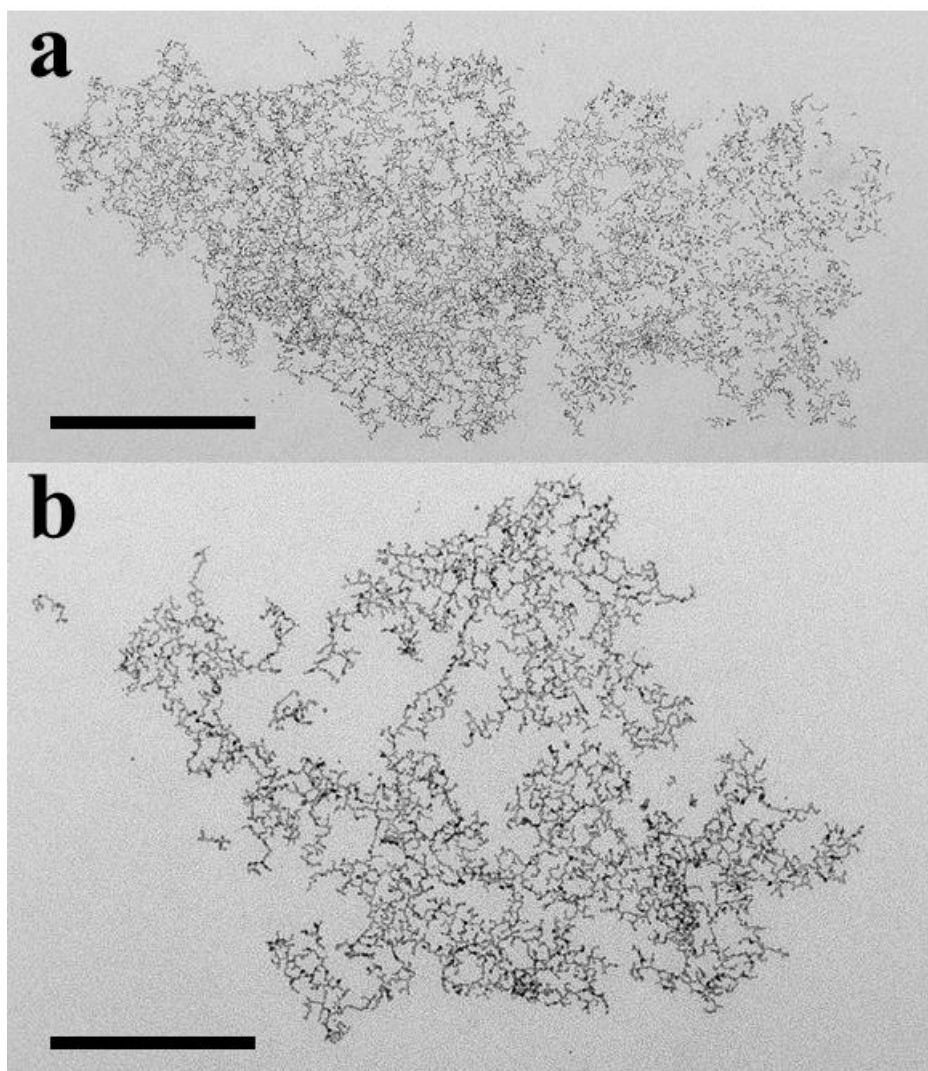


Figure S4 TEM images of Ir nanorods at (a) low and (b) high magnifications. The scale bars in (a) and (b) are 200 nm and 100 nm, respectively.

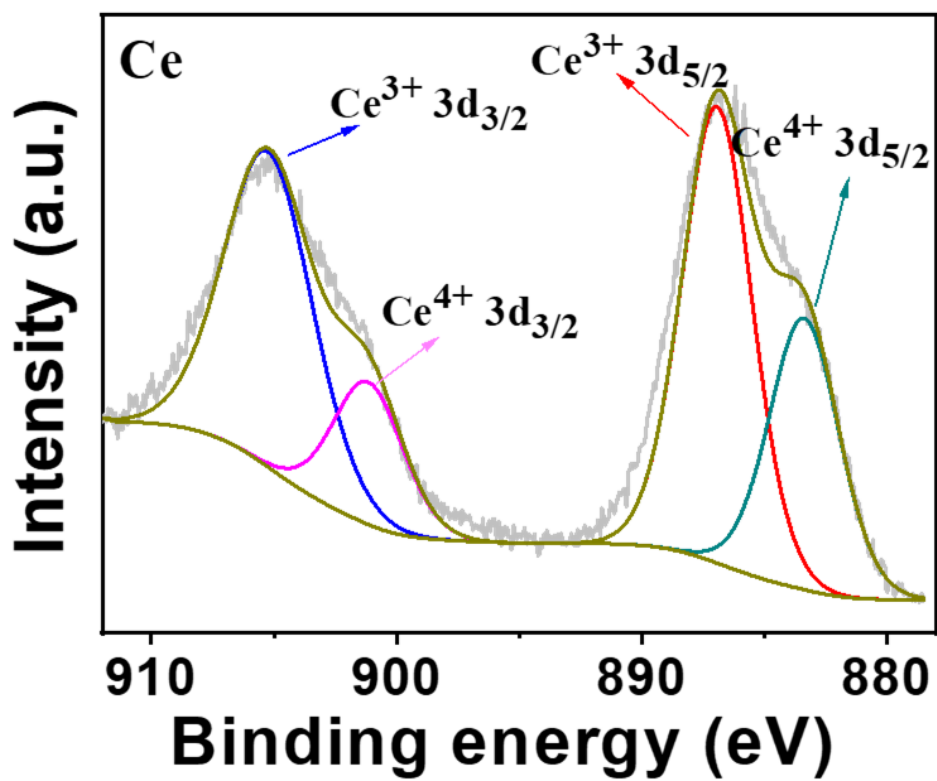


Figure S5 XPS spectra of Ce in Ir/CeO₂

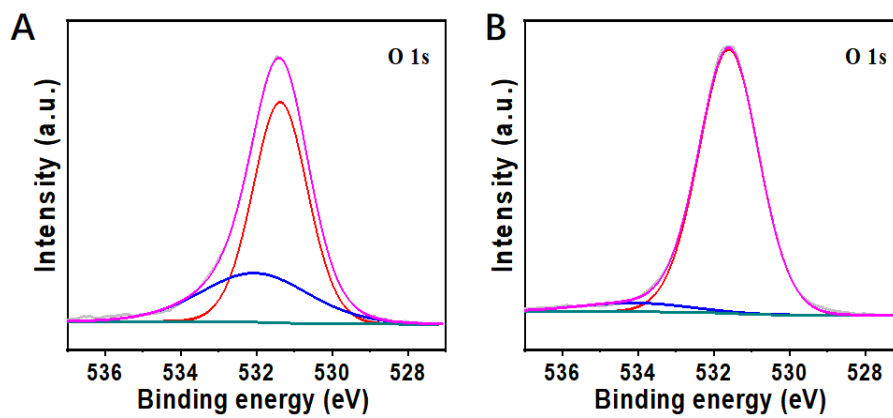


Figure S6 The High-resolution O 1s XPS spectra of (A) Ir/CeO₂ and (B) Ir.

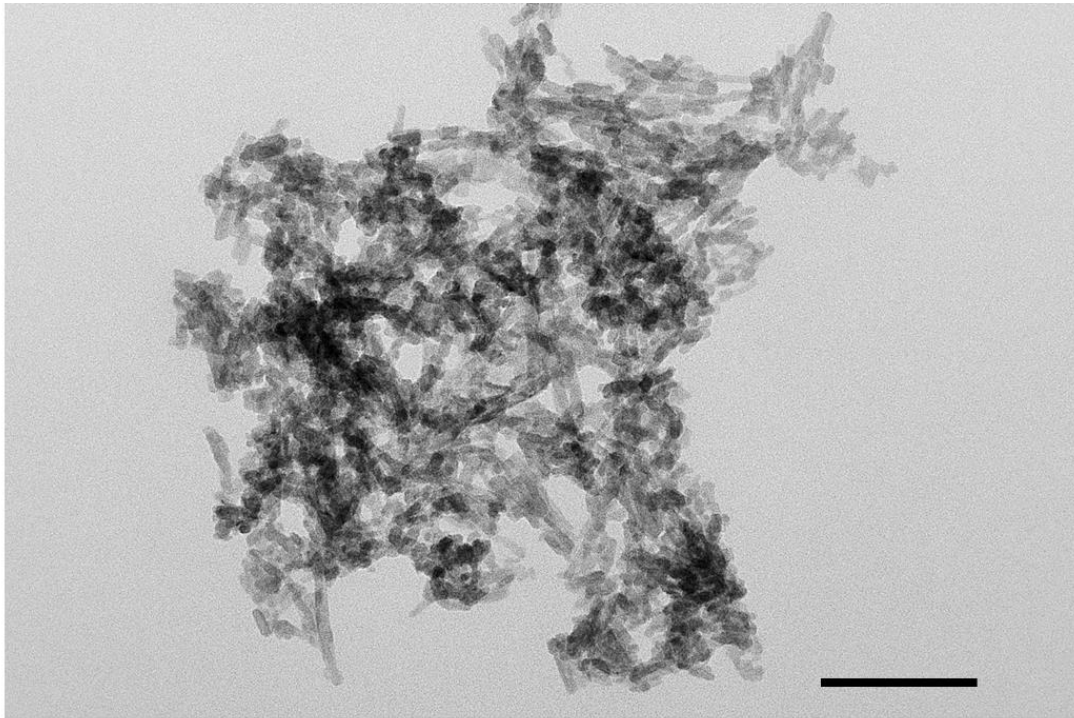


Figure S7 TEM image of CeO₂ prepared in the same process. The scale bar is 100 nm.

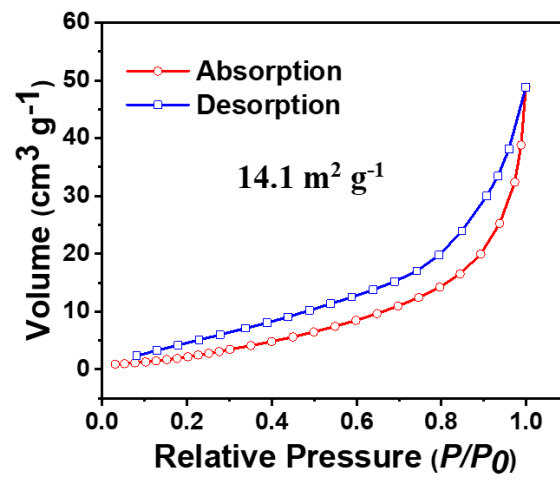


Figure S8 Nitrogen adsorption-desorption isotherms of Ir/CeO₂. The BET area is 14.1 $\text{m}^2 \text{g}^{-1}$.

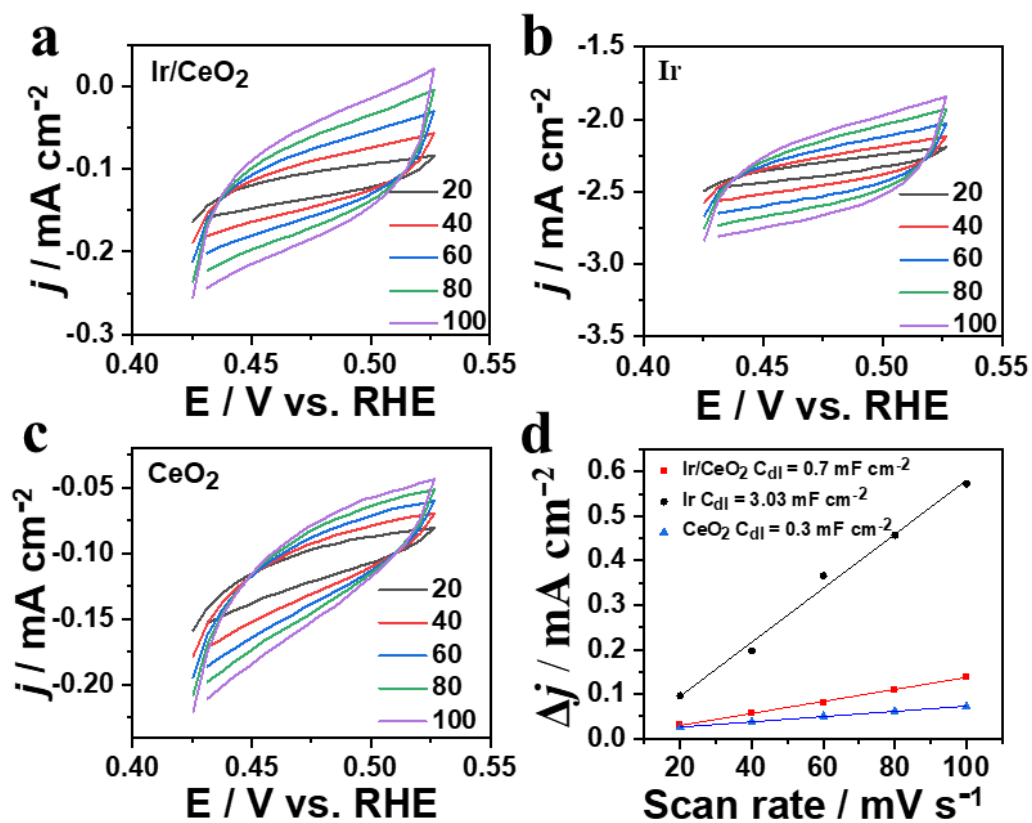


Figure S9 CV curves of (a) Ir/CeO₂, (b) Ir nanorod, (c) CeO₂ at various scanning rate, (d) the corresponding C_{dl} . Ir/CeO₂ displays a small EASA, nearly one quarter that of Ir nanorod.

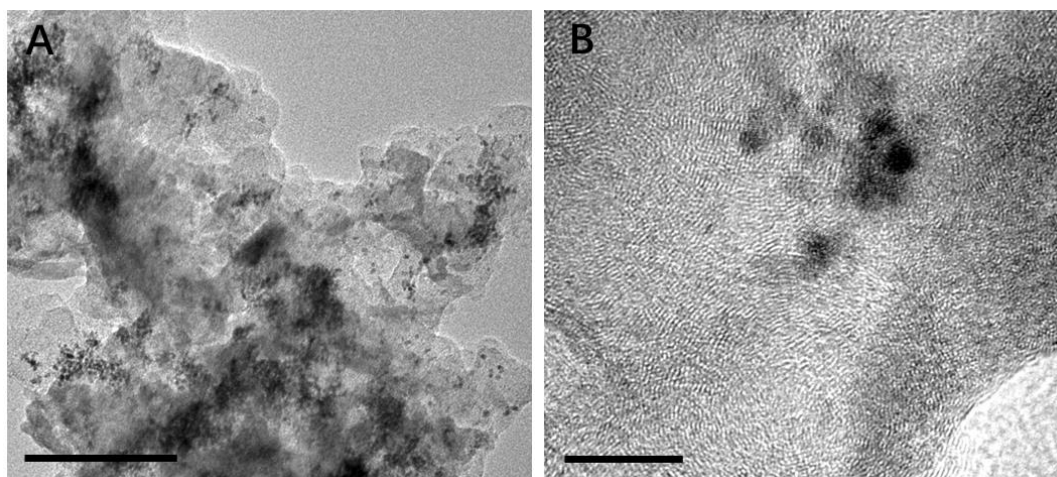


Figure S10 TEM images at (A) low and (B) high magnifications of Ir/CeO₂ after OER durability test. The scale bars in (A) and (B) are 100 nm and 10 nm, respectively.

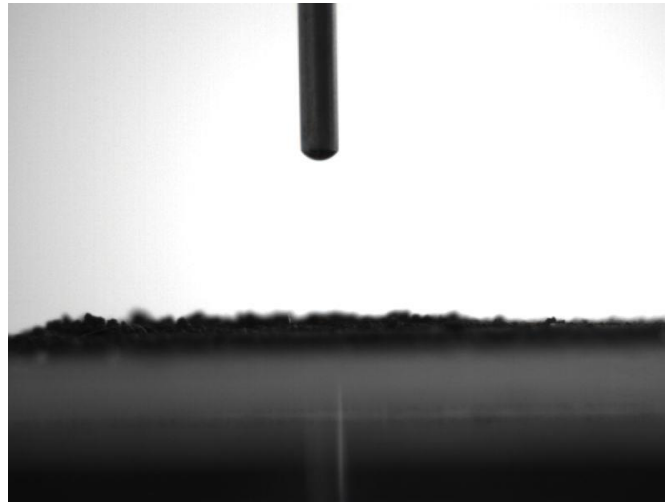


Figure S11 The contact angle of Ir/CeO₂.

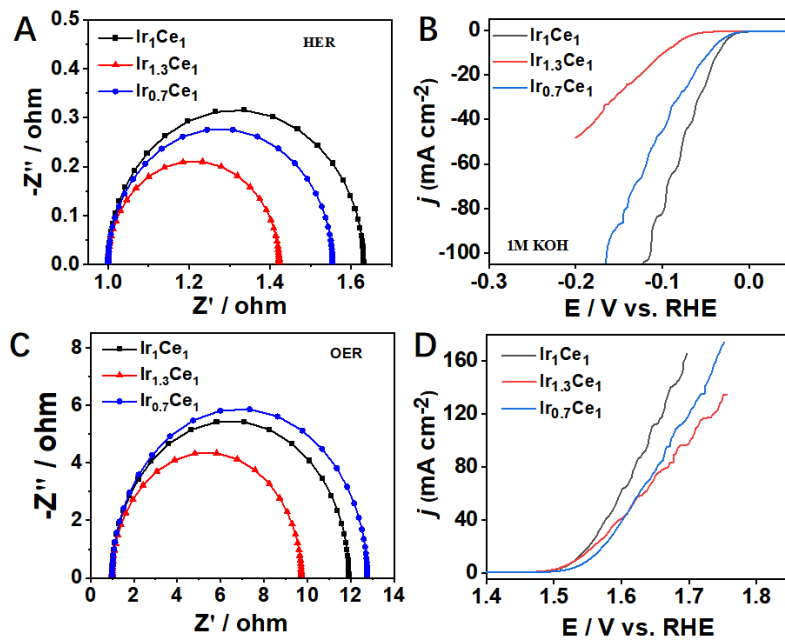


Figure S12 (A) EIS spectra and (B) HER polarization curves, (C) EIS spectra and (D) OER polarization curves of Ir/CeO₂ with different Ir content.

Table S1 The catalysts with different Ir content.

Samples	Precursor /mg		Content Based on ICP/ atom.%	
	IrCl ₃ ·xH ₂ O	CeCl ₃ ·7H ₂ O	Ir	Ce
Ir1Ce1	20	30	43.4	56.6
Ir1.3Ce1	26	30	49.6	50.4
Ir0.7Ce1	14	30	31.2	68.8

Table S2 Comparison of HER performance in the literature.

Catalysts	η_{10} mV	Solution	Ref.
Ir/CeO ₂	36	1.0 M KOH	This work
Rh nanosheets	43	1.0 M KOH	3
Rh-Rh ₂ P	37	1.0 M KOH	4
Rh/SWNTs	48	1.0 M KOH	5
Rh ₆ Cu ₁ NPs	36	1.0 M KOH	6
CoP	62.5	1.0 M KOH	7
Co ₉ S ₈ @MoS ₂	143	1.0 M KOH	8
Ir ONAs	47	0.1 M KOH	9
IrCo@NC	45	1.0 M KOH	10
Ir-OMC	80	0.1 M KOH	11

Table S3 Comparison of OER performance in the literature.

Catalysts	η_{10} mV	Solution	Ref.
Ir/CeO ₂	300	1.0 M KOH	This work
Rh nanosheets	360	1.0 M KOH	3
Rh tetrahedrons	415	1.0 M KOH	
Rh concave tetrahedrons	464	1.0 M KOH	
CoP	330	1.0 M KOH	7
Co ₉ S ₈ @MoS ₂	342	1.0 M KOH	8
IrO ₂	353	1.0 M KOH	12

References

1. Y. Zhang, C. Wu, H. Jiang, Y. Lin, H. Liu, Q. He, S. Chen, T. Duan and L. Song, *Adv. Mater.*, 2018, **30**, e1707522.
2. H.-P. Guo, B.-Y. Ruan, W.-B. Luo, J. Deng, J.-Z. Wang, H.-K. Liu and S.-X. Dou, *ACS Catalysis*, 2018, **8**, 9686-9696.
3. N. Zhang, Q. Shao, Y. Pi, J. Guo and X. Huang, *Chem. Mater.*, 2017, **29**, 5009-5015.
4. F. Luo, L. Guo, Y. Xie, J. Xu, W. Cai, K. Qu and Z. Yang, *J. Mater. Chem. A*, 2020, **8**, 12378-12384.
5. W. Zhang, X. Zhang, L. Chen, J. Dai, Y. Ding, L. Ji, J. Zhao, M. Yan, F. Yang, C.-R. Chang and S. Guo, *ACS Catal.*, 2018, **8**, 8092-8099.
6. W. Zhang, J. Zhao, J. Zhang, X. Chen, X. Zhang and F. Yang, *ACS Appl. Mater. Interfaces*, 2020, **12**, 10299-10306.
7. H. Li, Q. Li, P. Wen, T. B. Williams, S. Adhikari, C. Dun, C. Lu, D. Itanze, L. Jiang, D. L. Carroll, G. L. Donati, P. M. Lundin, Y. Qiu and S. M. Geyer, *Adv. Mater.*, 2018, **30**, 1705796.
8. J. Bai, T. Meng, D. Guo, S. Wang, B. Mao and M. Cao, *ACS Appl. Mater. Interfaces*, 2018, **10**, 1678-1689.
9. F. Yang, L. Fu, G. Cheng, S. Chen and W. Luo, *J. Mater. Chem. A*, 2017, **5**, 22959-22963.
10. P. Jiang, J. Chen, C. Wang, K. Yang, S. Gong, S. Liu, Z. Lin, M. Li, G. Xia, Y. Yang, J. Su and Q. Chen, *Adv Mater*, 2018, **30**.
11. Y. He, J. Xu, F. Wang, X. Zhao, G. Yin, Q. Mao, Y. Huang and T. Zhang, *Journal of Energy Chemistry*, 2017, **26**, 1140-1146.
12. W. Zhong, Z. Lin, S. Feng, D. Wang, S. Shen, Q. Zhang, L. Gu, Z. Wang and B. Fang, *Nanoscale*, 2019, **11**, 4407-4413.